A methodology based on 2.5D FEM-BEM for the evaluation of the vibration energy flow radiated by underground railway infrastructures

Dhananjay Ghangale[a,*], Robert Arcos[a,d,e], Arnau Clot[b], Julen Cayero[c], Jordi Romeu[a]

[a] *Acoustical and Mechanical Engineering Laboratory (LEAM), Universitat Politècnica de Catalunya (UPC). c/ Colom, 11, 08222 Terrassa (Barcelona), Spain.*

[b] *Department of Engineering, University of Cambridge, United Kingdom*

[c] *Departamento de Ingeniería de Sistemas, Automática e Informática Industrial (ESAII), Universitat Politècnica de Catalunya (UPC). c/ Colom, 11, 08222 Terrassa (Barcelona), Spain.*

[d] *CONSTRUCT, Faculty of Engineering (FEUP), University of Porto. Rua Dr. Roberto Frias, Porto 4200-465, Portugal.*

[e] *Serra Húnter Fellow, Universitat Politècnica de Catalunya (UPC).*

Abstract

In this paper, a comprehensive numerical approach for modelling track/tunnel/soil systems in the context of ground-borne railway-induced vibration problems considering a full-space model of the soil is proposed. All the approach is formulated in the wavenumber-frequency domain and it consists of a coupled

*Corresponding author

Email addresses: dhananjay.ghangale@upc.edu (Dhananjay Ghangale), robert.arcos@upc.edu (Robert Arcos)

finite element-boundary element model of the tunnel/soil system, a semi-analytical model of the track, a multibody model for the vehicle and a model for the vibration propagation in the soil based on semi-analytical solutions of a cylindrical cavity in a full-space. This comprehensive approach has been developed with the aim of computing the vibration energy flow radiated upwards by underground railway tunnels. An axisymmetric formulation to deal with circular underground railway tunnels is included in the approach in order to improve the computational speed of the methodology. This formulation can also be used for other types of railway tunnels if a circular boundary of the boundary element mesh is considered. Since this methodology uses finite elements to model the tunnel structure, its modelling detail is higher than the previously developed methodologies dedicated to compute the vibration energy flow radiated by underground railway infrastructures, since they are based on semi-analytical modelling of the tunnel structure. The present methodology has been specifically designed to be used in general assessment studies about ground-borne underground railway-induced vibrations where decisions on the type of track and/or the application of mitigation measures at the source, as soft rail-pads, under-ballast or under-slab mats have to be made. Moreover, this methodology can be used for the study of the vibration radiation patterns of railway tunnels.

Keywords: Railway-induced vibration, Railway tunnels, 2.5D, Coupled FEM-BEM, Vibration energy flow

---

1. Introduction

Noise and vibration pollution in urban areas is a major issue of concern for governments and administrations due to the increasing preoccupation by the general population about the effects on their comfort and quality of life. One of the most important sources that cause this contamination is railway traffic. Ground-borne vibration is perceived as mechanical vibration of the human body in a relevant frequency range from 1 Hz to 80 Hz and ground-borne noise (also known as re-radiated noise) is perceived as a sound emitted by the building structure in a relevant frequency range from 16 Hz to 250 Hz [1]. Since almost all developed regions of the world have laws to regulate the maximum levels of noise and vibration to which the population is exposed, predictions of these levels must be carried out in designing new railway infrastructures or when new buildings are planned to be constructed near existing railway tracks.

A comprehensive overview of the state of the art on railway-induced ground-borne vibration concerning governing physical mechanisms, prediction methods and mitigation measures has been presented by Lombaert et al. [2]. These prediction approaches are of three kinds: empirical, analytical and numerical [3]. Empirical models are based on measurements performed on specific sites and, thus, in the majority of cases, are not usually suitable for predictions of noise and vibration induced by new infrastructures. In general, analytical and numerical approaches are the most commonly used methodologies when a medium/high level of accuracy is required. These modelling techniques are commonly used for the design of vibration mitigation measures [4, 5, 6, 7, 8].

Comprehensive models of the complete system related to underground railway-induced vibration problems should account for the vehicle, the track, the tunnel, the ground and the building. A methodology that uses a two-dimensional (2D) finite element (FE) model to predict train-induced vibrations in a building was first proposed by Balendra et al. [9, 10] and Chua et al. [11]. However, 2D models do not take into account the wave propagation in the direction of the track and, even more important, they cannot account for the train motion along the track [12]. Hunt [13, 14] presented an analytical-stochastic methodology to calculate ground-borne vibration in buildings due to underground railway traffic in a three-dimensional (3D) point of view. Weak coupling between the incident wave field due to the railway traffic and the building structure was assumed. This incident wave field was calculated considering a stochastic modelling of the vibration generation and propagation mechanisms [15]. Fiala et al. [16] developed a 3D methodology to calculate the ground-borne vibration and re-radiated noise on buildings for the case of at-grade infrastructures, based on a FE model of the building structure coupled with a boundary element (BE) model of the layered ground [17]. Later, Fiala et al. [18], in order to take into account the track longitudinal variability, used the well-established 3D periodic finite element method (FEM) and boundary element method (BEM) model, previously developed by Clouteau et al. [19], for the computation of the free field ground surface displacements induced by the vehicle/superstructure/tunnel/ground system.

Another relevant approach that is able to calculate the incident wave field due to railway traffic in a 3D point of view is the two-and-a-half-dimensional (2.5D) FEM-BEM modelling scheme [20], which reduces the meshing pro-

blem to a 2D one but considers the track/tunnel system to be longitudinally invariant. This methodology is being widely used nowadays, giving accurate results in the prediction of ground-borne vibration [12, 21, 22]. Recent investigations [23, 24] have proposed significant improvements of this methodology by using a regularised boundary integral as an alternative to the evaluation of the singular integrals which appear in the 2.5D BE formulation and by considering the Green's functions of a layered half-space [25] leading the latter to very significant simplifications of the meshing problem. Jin et al. [26] validated the 2.5D FEM-BEM approach with experimental measurements. Lopes et al. [27] proposed a methodology using FEM and perfectly matched layers (PML) to model the wave propagation in the soil to study soil-structure interaction problem. An alternative methodology was proposed by Amado-Mendes et al. [28], which uses the method of fundamental solution (MFS) instead of PML. Yaseri et al. [29] proposed a method based on FE coupled with scaled boundary finite elements, to study the ground vibration of underground railways.

Rather than accounting for the complete system, considering only a model for the vehicle/track/tunnel/soil system that accounts for the surrounding soil as a full-space is a computationally efficient approach for the evaluation of vibration mitigation measures applied on the source. In this regard, vibration energy flow is a tool that can be used in designing effective countermeasures for reducing the vibration generated by underground railway infrastructures. Hussein and Hunt [30] proposed a power flow study based on the PiP model of Forrest and Hunt [31] and Hussein and Hunt [32]. The model was later improved by Hussein et al. [33] by replacing the initial full-space model of

the soil with a layered half-space. In order to obtain vibration power flow radiated by double-deck tunnel Clot et al. [34, 35] proposed a model of a tunnel structure which couples a longitudinally infinite plate, as a model of the interior floor, with the PiP model. A limitation of the methodologies for computing power flow previously mentioned is that power flow can be obtained from only simple geometrical configurations of underground tunnel systems. This paper in contrast presents a methodology to compute the vibration energy flow from underground railway infrastructures that allows for a detailed modelling of tunnel structures.

In this context, this work proposes a computationally efficient method based on a 2.5D FEM-BEM approach that allows for the prediction of railway-induced vibration and vibration energy flow radiated by underground railway infrastructures. With respect to PiP, the present approach is able to accurately define the tunnel geometry since a 2.5D FEM-BEM approach is used in the present methodology to model the tunnel/soil system. As a benifit with respect to previously developed 2.5D FEM-BEM approaches intended to deal with underground railway-induced ground-borne vibration problems [20, 36, 23], the present approach is able to:

- Easily obtain the tractions on the soil, which are required to compute the radiated energy flow.
- Efficiently compute the displacements and traction in a large set of evaluation points (referred to as evaluators from here on) in the soil, which is another requirement of the energy flow calculations. This is

accomplished thanks to the use of the semi-analytical solutions of a cavity embedded in a full-space as a model of the soil.

Moreover, the computational efficiency of the 2.5D FEM-BEM approach itself is improved in the present methodology by the application of two strategies for faster computation of 2.5D BEM matrices. Firstly, the axisymmetry of most railway tunnel infrastructures is exploited in order to reduce the amount of soil Green's functions evaluations. This formulation can also be used for other types of railway tunnels if a circular boundary of the BE mesh is considered. Secondly, it is proposed to use a uniform distribution of BE nodes which, combined with the assumption of homogeneous full-space model of the soil, results in a significant reduction of the unique set of relative distances at which the Green's functions of the soil should be evaluated. Finally, an efficient sampling strategy for obtaining an accurate response of the system due to a train pass-by excitation is presented. A comparative study of the energy flow radiated by a tunnel with a track based on direct fixation rail fastening system (DFF) and a tunnel with a floating slab track (FST) is presented as an application of this methodology.

2. Numerical methodology

As previously stated, the aim of this paper is to present a new methodology for the computation of vibration energy flow radiated in the soil by train traffic through railway tunnels. The global computation scheme of the methodology is shown in Fig. 1. This computation scheme consists of

four different models: the track/tunnel/soil model, the train/track interaction model, the train pass-by response model and the vibration energy flow computation.

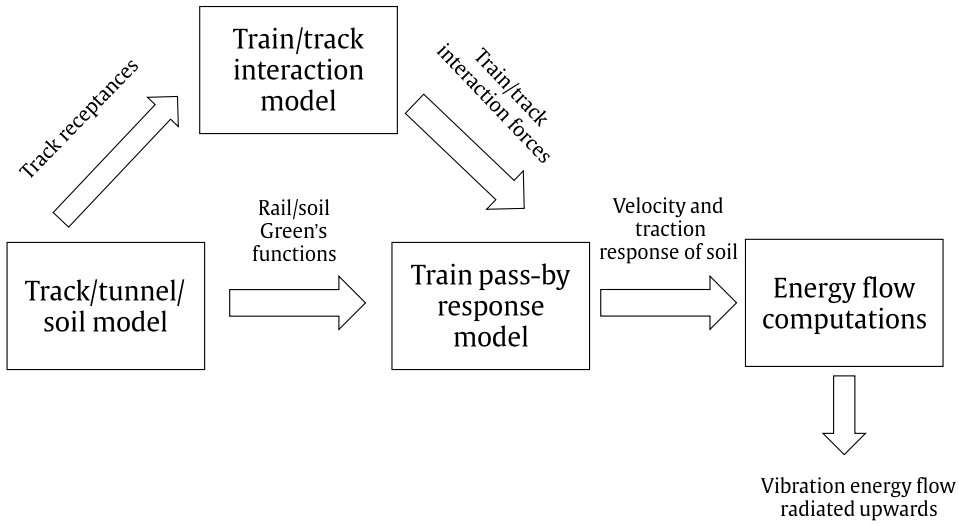

Fig. 1: Schematic description of the methodology.

The track/tunnel/soil system consists of three models: a semi-analytical model of the track, a model based on a 2.5D FEM-BEM approach for the tunnel/soil system and the semi-analytical solutions of a cylindrical cavity in a full-space as a model of the vibration propagation in the soil. In the semi-analytical model of the track, the rails are modelled as Euler-Bernoulli beams and the fasteners as longitudinally distributed linear viscous springs. Tunnel/soil modelling is accomplished by a 2.5D FEM-BEM wherein the tunnel structure is modelled by FE and the local surrounding soil is modelled with BE.

A description of the 2.5D FEM-BEM model used in this work can be found in [37]. The connection between the tunnel/soil model and the semi-analytical solutions of the cylindrical cavity is made through displacements compatibility on the tunnel/soil interface, which are obtained with the 2.5D FEM-BEM model of the tunnel/soil system. These displacements are used as boundary conditions in the semi-analytical solutions of the cavity in order to obtain the displacements and the tractions at arbitrary points in the soil. The semi-analytical solutions of a cavity in a full-space can be found in [34, 31, 38]. The train-track interaction and the train pass-by models used in the present study considers a fully 2D version of the models described by [39].

As shown in the Fig. 1, the coupled model of the train/track/tunnel/soil system is solved in two steps. In the initial step, the track receptances in the moving frame of reference obtained by the 2.5D FEM-BEM model are used together with the train/track interaction model to compute the wheel/rail interaction forces in the frequency domain. In the next step, the wheel/rail interaction forces and the Green's functions of the system for forces on the rails and the responses on soil (or other points on the system where the vibration response due to a train pass-by is desired to be computed) are used together in the train pass-by response model to obtain the vibration and/or tractions response in selected evaluators. Finally, the vibration energy flow can be obtained in the soil by using the velocity and traction responses in a set of points located in the soil around the tunnel. The train/track interaction model mainly consists of a rigid multibody model of the vehicle and a wheel/rail contact model based on Hertz contact theory.

In this paper, vectors are denoted by upper case bold italic letters and matrices and tensors are represented by upper case upright bold letters. Variables in the frequency domain are denoted by capital letters, bar notation is used to denote variables in the wavenumber domain and tilde notation is used to denote variables in wavenumber-frequency domain seen from the point of view of the moving frame of reference that follows the train motion.

2.1. Verification of the tunnel/soil model

In this section, the verification of the numerical methodology to obtain the tractions in the soil is presented. The verification is done in the basis of a system consisting of a cylindrical cavity in a homogeneous full-space. A cavity radius r_t of 1 m is considered and the mechanical parameters of the full-space are presented in Table 1. Two models of this system are compared in this verification: on one hand, the semi-analytical solutions of a cylindrical cavity in a full-space provided by Gazis [38] constitute the reference solution; on the other hand, an equivalent 2.5D FEM-BEM model of this cavity in a full-space system has been constructed meshing a region close to the cavity with finite elements and the rest with boundary elements. The region considered for 2.5D FEM mesh is a circular ring of 0.2 m thickness meshed with linear triangular elements. The outer boundary of the circular ring has been meshed by 80 linear boundary elements. Displacements at the nodes of the boundary elements are used as boundary conditions for the vibration propagation model in the soil.

Parameters	Notation	Units	Value
Young's modulus	E	[MPa]	108
Poisson ratio	ν	[−]	0.334
Density	ρ	[kg/m^3]	1800
Damping	$D_p = D_s$	[−]	0.025

Table 1: Properties of full-space used in the verification.

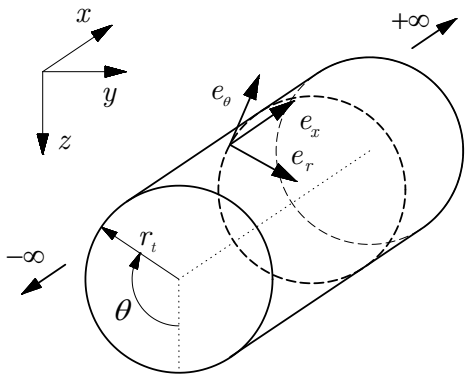

Fig. 2: Cylindrical cavity in a full-space. Definition of the Cartesian and cylindrical coordinate systems for both semi-analytical and 2.5D FEM-BEM models.

For both the models, the traction Green's functions due to a vertical force applied at the inner boundary of the cavity and at $\theta = 0$ are computed for frequencies up to 100 Hz and for wavenumbers from -2π rad/m to 2π rad/m. Tractions are computed by both models for evaluators located at a radial distance of 2 m from the centre of the cavity and placed at angular locations θ of 0, $\pi/2$ rad, π rad and $3\pi/2$ rad. Figure 3 shows the results of the radial tractions obtained by both models at all evaluators previously defined. From these results, it can be concluded that there is a very good agreement between the results obtained with the proposed numerical methodology and the reference theoretical solution. This implies that the numerical

methodology used in the framework of this article is properly verified. There is, however, a slight mismatch in the results between the two methods at certain frequencies. Apart from the intrinsic errors related to the nature of mesh, the slight mismatch comes from the number of ring modes considered [31] and the approximation done in the context of the 2.5D FEM model of the tunnel to approach a theoretical point load.

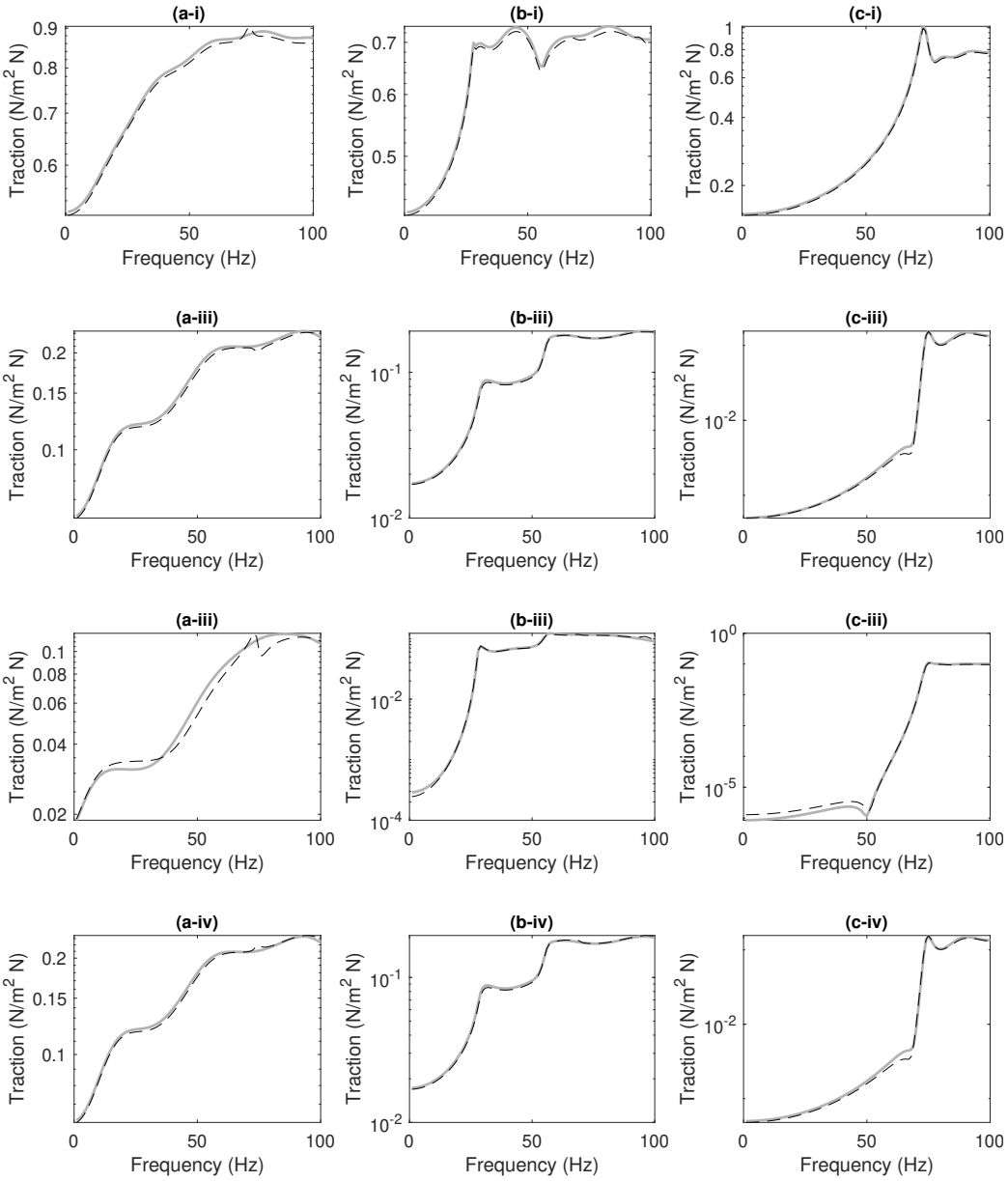

Fig. 3: Green's functions of the radial tractions obtained by the numerical methodology presented in this paper (dashed black line) and the semi-analytical model of a cavity in a full-space (grey solid line). The results are obtained at evaluators placed at a radius of 2 m and at angular positions of 0 rad (i) $\pi/2$ rad (ii) π degrees (iii) and $3\pi/2$ rad (iv). The results are associated to the wavenumbers of 0 (a), $\pi/2$ rad/m (b) and π rad/m (c).

2.2. Track model and its coupling with the tunnel structure

In the methodology used in this paper, it is proposed to use a semi-analytical model of the track coupled with a 2.5D FEM-BEM model of the tunnel/soil system. In this semi-analytical model of the track, the rails are modelled as two identical Euler-Bernoulli beams of infinite length and the fasteners are modelled as continuously distributed linear massless viscous springs. Both rails and all the fasteners are considered to have the same mechanical parameters, being E_r the Young's modulus of the rail material, I_r the second moment of inertia of the rail cross section, ρ_r the density of the rail material, S_r the rail cross-sectional area and k_f and c_f are the stiffness and viscous damping of the fasteners, respectively. Thus, the expression that defines the dynamic behaviour of the rails excited by moving harmonic vertical point loads with the same excitation frequency $\tilde{\omega}$ and the same speed v_t can be expressed in the wavenumber-frequency domain as

$$[E_r I_r k_x^4 - \rho_r S_r \omega^2]\bar{\boldsymbol{Z}}_r + (k_f + \mathrm{i}\omega c_f)(\bar{\boldsymbol{Z}}_r - \bar{\boldsymbol{Z}}_{tr}) = 2\pi\delta(\tilde{\omega} - (\omega + k_x v_t))\bar{\boldsymbol{F}}_r, \quad (1)$$

where $\bar{\boldsymbol{Z}}_r = \{\bar{Z}_{r_1}\ \bar{Z}_{r_2}\}^T$ are the vertical displacements of the first and second rails and $\bar{\boldsymbol{Z}}_{tr} = \{\bar{Z}_{tr_1}\ \bar{Z}_{tr_2}\}^T$ are the equivalent vertical displacements of the tunnel below the first and second rails. These equivalent vertical displacements are obtained by averaging the direct and cross responses of the FE nodes of the tunnel that are virtually in contact of the base plates of the physical rail fasteners. The response of the tunnel below the rails is given by

$$\bar{\boldsymbol{Z}}_{tr} = \bar{\mathbf{H}}_{tr}^{tr}\bar{\boldsymbol{F}}_{tr}, \quad (2)$$

where $\bar{\boldsymbol{F}}_{tr} = \{\bar{F}_{tr_1}\ \bar{F}_{tr_2}\}^T$ are the equivalent vertical forces applied on the system below first and second rails and $\bar{\mathbf{H}}_{tr}^{tr}$ are the Green's functions that relate the equivalent vertical displacements of the tunnel below the rails with the equivalent vertical forces applied also there. These Green's functions can be obtained by the 2.5D FEM-BEM model of the tunnel/soil described in the previous section. Moreover, the forces $\bar{\boldsymbol{F}}_{tr}$ can be expressed in terms of the displacements of the rails and the equivalent vertical displacements of the tunnel below the rails as shown in Eq. (1) as

$$\bar{\boldsymbol{F}}_{tr} = (k_f + \mathrm{i}\omega c_f)(\bar{\boldsymbol{Z}}_r - \bar{\boldsymbol{Z}}_{tr}). \tag{3}$$

Combining Eqs. (2) and (3), the relation between the displacements of the rails and the equivalent vertical displacements of the tunnel below the rails can be written as

$$\bar{\boldsymbol{Z}}_{tr} = \left(\frac{1}{k_f + \mathrm{i}\omega c_f}\mathbf{I} + \bar{\mathbf{H}}_{tr}^{tr}\right)^{-1} \bar{\mathbf{H}}_{tr}^{tr}\bar{\boldsymbol{Z}}_r. \tag{4}$$

Inserting Eq. (4) in Eq. (1), the response of the rails can be written as

$$\left[(E_r I_r k_x^4 - \rho_r S_r \omega^2)\mathbf{I} + \bar{\mathbf{K}}_{ft}\right] \bar{\boldsymbol{Z}}_r = 2\pi\delta(\tilde{\omega} - (\omega - k_x v))\bar{\boldsymbol{F}}_r, \tag{5}$$

where,

$$\bar{\mathbf{K}}_{ft} = (k_f + \mathrm{i}\omega c_f)\left[\mathbf{I} - \left(\frac{1}{k_f + \mathrm{i}\omega c_f}\mathbf{I} + \bar{\mathbf{H}}_{tr}^{tr}\right)^{-1} \bar{\mathbf{H}}_{tr}^{tr}\right]. \tag{6}$$

Thus, the Green's functions of the vertical displacements of the rails due vertical forces on them in the moving frame of reference $\tilde{\mathbf{H}}_r^r$ are given by

$$\tilde{\mathbf{H}}_r^r = \left[\left[E_r I_r k_x^4 - \rho_r S_r \left(\tilde{\omega} + k_x v_t \right)^2 \right] \mathbf{I} + \tilde{\mathbf{K}}_{ft} \right]^{-1}, \tag{7}$$

where $\tilde{\mathbf{K}}_{ft} = \tilde{\mathbf{K}}_{ft}(k_x, \tilde{\omega}) = \bar{\mathbf{K}}_{ft}(k_x, \tilde{\omega} + k_x v_t)$.

Then, the Green's functions that relate the response of the tunnel/soil system coupled with rails due to the vertical forces on the rails in the moving frame of reference $\tilde{\mathbf{H}}_s^r$ are given by

$$\tilde{\mathbf{H}}_s^r = \tilde{\mathbf{H}}_s^{tr} \tilde{\mathbf{K}}_{ft} \tilde{\mathbf{H}}_r^r, \tag{8}$$

being

$$\tilde{\mathbf{H}}_s^r = \left\{ \tilde{\mathbf{H}}_s^{r_1} \quad \tilde{\mathbf{H}}_s^{r_2} \right\}, \quad \tilde{\mathbf{H}}_s^{tr} = \left\{ \tilde{\mathbf{H}}_s^{tr_1} \quad \tilde{\mathbf{H}}_s^{tr_2} \right\}, \tag{9}$$

where $\tilde{\mathbf{H}}_s^{tr}$ are the Green's functions of the tunnel/soil system due to forces applied below the rails, which can be obtained using the 2.5D FEM-BEM approach presented in the previous section considering that $\tilde{\mathbf{H}}_s^{tr} = \tilde{\mathbf{H}}_s^{tr}(k_x, \tilde{\omega}) = \bar{\mathbf{H}}_s^{tr}(k_x, \tilde{\omega} + k_x v_t)$. In case that external mitigation measures are desired to be applied on the system, they can be coupled to the tunnel/soil system in the same way that rails are. For these cases, the Green's function of the system due to external forces applied at any arbitrary position of the tunnel/soil in the presence of the rails $\bar{\mathbf{H}}_s^{er}$ can be written as

$$\bar{\mathbf{H}}_s^{er} = \bar{\mathbf{H}}_s^{e} + k_{ft}^{e} \bar{\mathbf{H}}_s^{tr} \bar{\mathbf{H}}_{tr}^{e}, \tag{10}$$

where the sub-index or super-index e represents the external loading and

$$k_{ft}^{e} = (k_f + \mathrm{i}\omega c_f)\left(\frac{k_f + \mathrm{i}\omega c_f}{E_r I_r k_x^4 - \rho_r S_r \omega^2 + k_f + \mathrm{i}\omega c_f} - 1\right), \tag{11}$$

where $\bar{\mathbf{H}}_s^e$ are the Green's functions of the tunnel/soil system due to external forces in the absence of the rails and $\bar{\mathbf{H}}_{tr}^e$ are the Green's functions of the response of the tunnel below the rails due to the external loads in the absence of the rails. Finally, the Green's functions associated to the response of the rails due to external loading can be written as

$$\bar{\mathbf{H}}_r^e = k_{fr}^e \bar{\mathbf{H}}_{tr}^e, \tag{12}$$

where

$$k_{fr}^e = \frac{k_f + \mathrm{i}\omega c_f}{E_r I_r k_x^4 - \rho_r S_r \omega^2 + k_f + \mathrm{i}\omega c_f}. \tag{13}$$

Eqs. (10) and (12) are not defined in the moving frame of reference because the external loads are not usually moving with the train. Again, the Green's functions $\bar{\mathbf{H}}_s^{tr}$, $\bar{\mathbf{H}}_s^e$ and $\bar{\mathbf{H}}_{tr}^e$ can be computed using the 2.5D FEM-BEM approach presented in the previous section.

2.3. Wavenumber-frequency sampling strategy

The accuracy of the train pass-by response simulated in the basis of the present methodology is strongly dependent on how the Green's functions of the system are sampled in the wavenumber and frequency domain. In the present section, a sampling scheme is proposed in order to obtain a more accurate response of the system on account of the train pass-by. This

sampling scheme proposes a linear sampling for moving frequencies and a non-uniform sampling scheme along the wavenumber that varies with the frequency. Note that, in this section, the frequency seen from the fixed frame of reference ω is called static frequency and the frequency seen from the moving frame of reference $\tilde{\omega}$ is called moving frequency.

As a first step of the sampling strategy, the moving frequencies of the system are determined. Initially the required maximum static frequency $\omega_{\max}$ and the length of the sampling vector for the frequency N_ω are defined. The maximum moving frequency $\tilde{\omega}_{\max}$ is computed using the relation $\tilde{\omega}_{\max} = \omega_{\max}(1 + v_t/c_{\min})$ [21], where v_t is the train speed and $c_{\min}$ is the minimum wave speed of the system. Theoretical wave speeds of corrosponding ideal systems are used to obtain and approximation of $c_{\min}$ for the specific model studied. The sampling for the moving frequency is then obtained by considering a linear distribution of N_w discrete values of the frequency from 0 to $\tilde{\omega}_{\max}$.

In the second step of the sampling strategy, the sampling for the wavenumber k_x is determined. Initially, a pre-sampling process is performed, where the Green's functions of the system are obtained for two moving frequencies: $\pi/2$ rad/s and $\tilde{\omega}_{\max}$. Dense sampling vectors of $N_{k_x}^{ps}$ samples for the wavenumber are used for these two frequencies. Considering those frequencies and the approximated wave speeds used in the $c_{\min}$ evaluation, a wavenumber limit for each of those two frequencies and for the i-th subsystem can be computed as $k_{xi}^{\lim} = \tilde{\omega}/c_i$, where c_i is the approximated wave speed of the i-th subsystem. The number of sub-systems existing in the model is N_{ss}. For each

sub-system and each frequency, a wavenumber sampling vector of $N_{k_x}^{ps}/N_{ss}$ samples is constructed. Half of these samples are linearly distributed from $-2k_{xi}^{\lim}$ to $2k_{xi}^{\lim}$ (always considering the 0), and the rest are logarithmically distributed from $2k_{xi}^{\lim}$ to 10^5 rad/m and from $-2k_{xi}^{\lim}$ to -10^5 rad/m. Then, all sampling vectors associated to the same frequency are combined in only one pre-sampling vector of $N_{k_x}^{ps}$ samples. Finally, the two pre-sampling vectors obtained are used to compute the Green's functions of the system at both frequencies.

The wavenumber limit until where most of the spectral content is confined is obtained for the each pre-sampling frequencies and each evaluator in the system. For specific evaluators, four wavenumber limits are computed: two with a tolerance of 10%, $k_{x_{\text{lin}}}^{\lim_u}$ and $k_{x_{\text{lin}}}^{\lim_d}$, and another two with a tolerance of 0.1% $k_{x_{\log}}^{\lim_u}$ and $k_{x_{\log}}^{\lim_d}$. Subscripts u and d are referred to the maximum and minimum frequencies used in the pre-sampling. The wavenumber limits $k_{x_{\text{lin}}}^{\lim_u}$, $k_{x_{\text{lin}}}^{\lim_d}$, $k_{x_{\log}}^{\lim_u}$ and $k_{x_{\log}}^{\lim_d}$ of only three evaluators are considered. These evaluators should be selected ensuring that they are representing high, medium and low wavenumber limits of all the evaluators of the system. It is assumed that the wavenumber limits $k_{x_{\text{lin}}}^{\lim}$ and $k_{x_{\log}}^{\lim}$ vary linearly along the moving frequency and, therefore, they can be expressed as a function of $\tilde{\omega}$ as

$$k_{x_{\text{lin}}}^{\lim}(\tilde{\omega}) = \left(\frac{\tilde{\omega} - \pi/2}{\tilde{\omega}_{\max} - \pi/2}\right)\left(k_{x_{\text{lin}}}^{\lim_u} - k_{x_{\text{lin}}}^{\lim_d}\right) + k_{x_{\text{lin}}}^{\lim_u} \tag{14}$$

and

$$k_{x_{\log}}^{\lim}(\tilde{\omega}) = \left(\frac{\tilde{\omega} - \pi/2}{\tilde{\omega}_{\max} - \pi/2}\right)\left(k_{x_{\log}}^{\lim_u} - k_{x_{\log}}^{\lim_d}\right) + k_{x_{\log}}^{\lim_u} \tag{15}$$

For each selected evaluator, a wavenumber sampling vector with a linear distribution of samples between $-k_{x_{\text{lin}}}^{\text{lim}}$ and $k_{x_{\text{lin}}}^{\text{lim}}$ (always considering the 0) and a logarithmic distribution from $k_{x_{\text{lin}}}^{\text{lim}}$ to $k_{x_{\text{log}}}^{\text{lim}}$ and from $-k_{x_{\text{lin}}}^{\text{lim}}$ to $-k_{x_{\text{log}}}^{\text{lim}}$ is constructed for each frequency. Half of the $N_{k_x}^s/3$ samples of this sampling vector (since N_{k_x} is the sampling vector length for the three evaluators combined) are used in the linear distribution and the other half in the logarithmic one. Finally, the non-uniform wavenumber sampling is obtained by combining the wavenumber samplings of the three selected evaluators.

3. Fast computation of elastodynamic BEM matrices

The computation of the stiffness matrix of soil involves the computation of the BEM matrices related to traction and displacement. In order to obtain these matrices, the computation of traction and displacement Green's functions for a set of source and evaluation points is required. For a BEM mesh, the source points are placed on the BE nodes and the evaluators are given by the Gaussian integration points along all the BE. Thus, the computation of BEM matrices involves the computation of the Green's function for all source/evaluator combinations. It is important to note that an increase in the number of BE increases the number of source points and evaluators and, thereby, the computational time of the BEM matrices calculation. In the method of François et al. [23] the Green's functions are computed on a grid of points and then an interpolation procedure is used to obtain the response at the required evaluators. However, interpolation could induce inaccurate results (with a sparse grid) or become computationally expensive

(with a dense grid). In the present work, all required Green's functions are computed in a computationally efficient way, avoiding the need of interpolation. Two strategies to accomplish this are discussed here. The first strategy can be applied to any problem geometry. It involves fast computation of Green's function and it is discussed in Sec. 3.1. The next strategy, discussed in Sec. 3.2, is only valid for a special class of problems encountered in underground railway infrastructures, specifically underground circular tunnels where the geometry of the BE mesh is axisymmetric.

3.1. Fast computation of the Green's functions in a full-space

As discussed previously, the computational time associated to the calculation of the tractions and displacements Green's functions depends on the amount of source and evaluators and on the number of discrete values for the wavenumber and the frequency. In a homogeneous full-space, the Green's functions are not a function of particular locations of the source and the evaluator: they are only a function of the relative distance between them. Relative distances between all source/evaluator combinations are contained in a smaller set of unique source/evaluator relative distances. Exploiting this fact, computing the Green's functions for this unique set of source/evaluator relative distances and then mapping them in order to obtain the Green's function for the complete set of source/evaluator combinations results in a faster procedure. This mapping also requires multiplying the Green's function with a transformation matrix that is described below. If all the BE of the BEM mesh have the same length, the number of unique set of source/evaluator

combinations distances is the smallest. Thus, in order to exploit all the benefits of the present methodology, it is proposed to design the BEM mesh ensuring that all the elements have the same length.

In order to perform the proposed procedure, it should be noted that the dependency of the displacement and tractions Green's functions on radial and angular coordinates can be separated into two functions: one only dependent on the relative radial distance and the other one only dependent on the relative angle. Taking this into account, the procedure to obtain the Green's function for any source/evaluator from the ones obtained at the unique set of source/ evaluator combination is as follows. Initially, the relative angles of all the source/evaluator combinations θ and the angles of the normals associated to all the evaluators ϕ are computed by

$$\phi = \arctan(n_y/n_z), \qquad \theta = \arctan(y/z), \tag{16}$$

where n_y and n_z are the normals and y and z are the relative distance in y and z directions. The normal are redefined as:

$$n_y = \cos(\phi - \theta), \quad n_z = \sin(\phi - \theta), \tag{17}$$

The displacement and traction Green's functions for the unique set source/evaluator relative distances, which are represented by $\bar{\mathbf{H}}_{us}$ and $\bar{\mathbf{T}}_{us}$, respectively, are obtained using the Green's function provided in [40] considering $z = 0$. Then the displacement Green's functions for the complete set of source/evaluators

can be obtained as:

$$\bar{\mathbf{H}} = \mathbf{T}_{\theta}^{-1}\mathcal{M}(\bar{\mathbf{H}}_{us})\mathbf{T}_{\theta} \tag{18}$$

where $\mathbf{T}_{\theta}$ is defined in Eq. (20) and $\mathcal{M}(.)$ represents the operation of the mapping from the unique set to complete set of source/evaluator combinations only in terms of relative distances. Similarly, the traction Green's functions can be obtained as

$$\bar{\mathbf{T}} = \mathbf{T}_{\theta}^{-1}(\mathcal{M}(\bar{\mathbf{T}}_{us}) \circ \mathbf{T}_{\phi})\mathbf{T}_{\theta} \tag{19}$$

where

$$\mathbf{T}_{\phi} = \begin{bmatrix} n_y & n_y & n_z \\ n_y & n_y & n_z \\ n_z & n_z & n_y \end{bmatrix} \qquad \mathbf{T}_{\theta} = \begin{bmatrix} 1 & 0 & 0 \\ 0 & \cos\theta & -\sin\theta \\ 0 & \sin\theta & \cos\theta \end{bmatrix} \tag{20}$$

and where $\circ$ represents the Hadamard product. In this paper, the Cartesian coordinates system considered is presented in Fig. 2.

3.2. Axisymmetric formulation

The axisymmetric nature of the soil/structure boundary in circular tunnels can be used to take advantage in reducing the computation costs related to the calculation of the BEM traction and displacements matrices. To exploit the axisymmetry of the boundary geometry, the BE must have the same length. In this case, the elements of the BEM matrices associated with all combinations of the sources and evaluators can be obtained from the elements associated with only one source. This is possible because each source sees the same pattern of evaluators locations, with relative rotation between them. Thus, if the elements associated to a reference source are computed, the

response for all the other combinations of source/evaluator distances can be easily obtained by multiplying these reference elements with a transformation matrix that takes into account the rotation between this reference source and the other ones. After this, appropriate mapping of the resulting elements should be performed. The transformation matrix having the relative rotation of the load points with respect to the axis of axisymmetry has the same form as $\mathbf{T}_\theta$ (mentioned in section 3.1) with angles θ that in this case are defined as the relative rotation between the required source points and the reference source point with respect to the axis of axisymmetry. The axisymmetric formulation is summarised as:

1. In a first step, all the BEM matrix elements for the reference source position and for all the evaluator locations are computed.

2. The elements for other source/evaluator locations for all wavenumbers are obtained from the elements obtained in the first step by multiplying the elements with a transformation matrix.

3. The transformation matrix is $\mathbf{T}_\theta$ in Eq. (20) with angles θ defined as the relative rotation between the required source points and the reference source point with respect to the axis of axisymmetry.

4. In the final step, appropriate mapping and assembly of the elements is performed to obtain the final required BEM matrices of tractions and displacements.

In cases of axisymmetric boundary geometries, the displacements and trac-

tions Green's functions are required to be computed only for the source points located on just one element, and then the mapping introduced in the Eq. (18) and Eq. (19) is required to performed once. Thus, the proposed axisymmetric formulation is further reducing the computation time required for BEM matrices evaluation.

4. Application example

In this section, the methodology described in the paper is applied with the aim of compare the vibration energy flow radiated by two different underground tunnel infrastructures. The underground railway infrastructures considered in this paper are a simple tunnel with a single track where the rails are directly attached to the tunnel invert (direct fastening system) and a simple tunnel with a floating slab track . For the sake of simplicity, the first tunnel system is called DFF and the second FST. A schematic of the DFF and FST models developed in this case study are shown in Figs. 4 and 5, respectively. The mechanical properties of these system are summarised in Table 2, for the DFF, and in Table 3, for the FST. For both models, the rails and the fasteners are modelled as proposed in section 2.2 and the properties for these systems used in the present case study are shown in Table 4.

The soil is modelled as a homogeneous full-space and the tunnels systems to be studied are embedded in it. Both the tunnels have an inner radius of 3 m and a wall thickness of 0.25 m. The tunnels are excited by vertical point loads at the points shown in blue star markers. These points are the

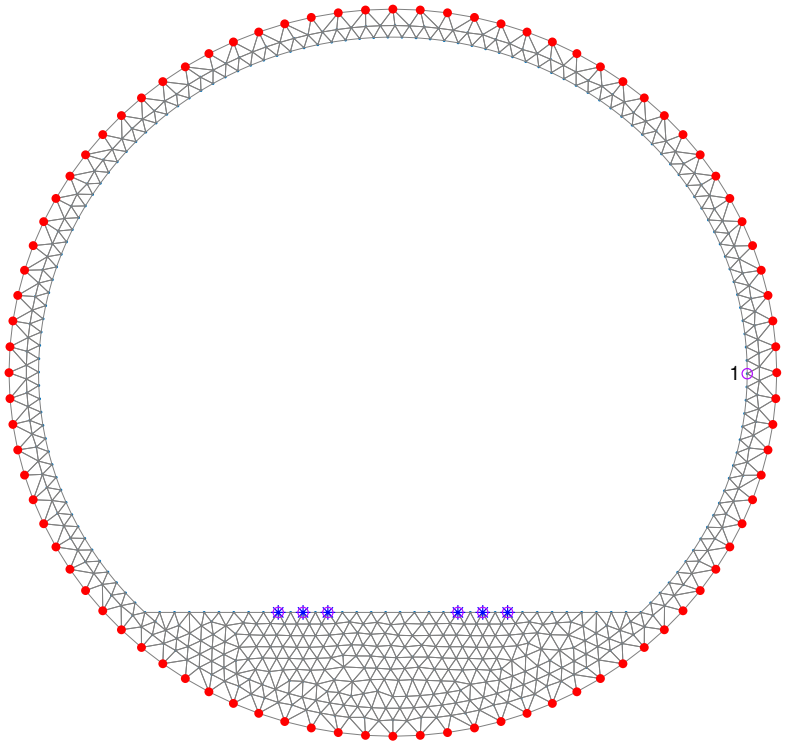

Fig. 4: Schematic of the DFF system modelled by 2.5D FE (tunnel) and BE (soil). Red solid markers represent the BE nodes, blue star markers are the points where forces are applied and pink circular markers denote the evaluators, where the evaluator in the tunnel wall is denoted by 1.

Subsystem	Parameters	Units	Value
Tunnel	Young's modulus	[GPa]	3.5
	Poisson ratio	[−]	0.15
	Density	[kg/m^3]	2500
	Damping	[−]	0.01

Table 2: Properties of DFF system.

points where the rails are coupled to the tunnel/soil system. The Green's functions of the track/tunnel/soil system for these point loads are obtained at the tunnel/soil interface (points shown in red) and evaluators locations (points shown in pink) using the method previously presented. Then, the

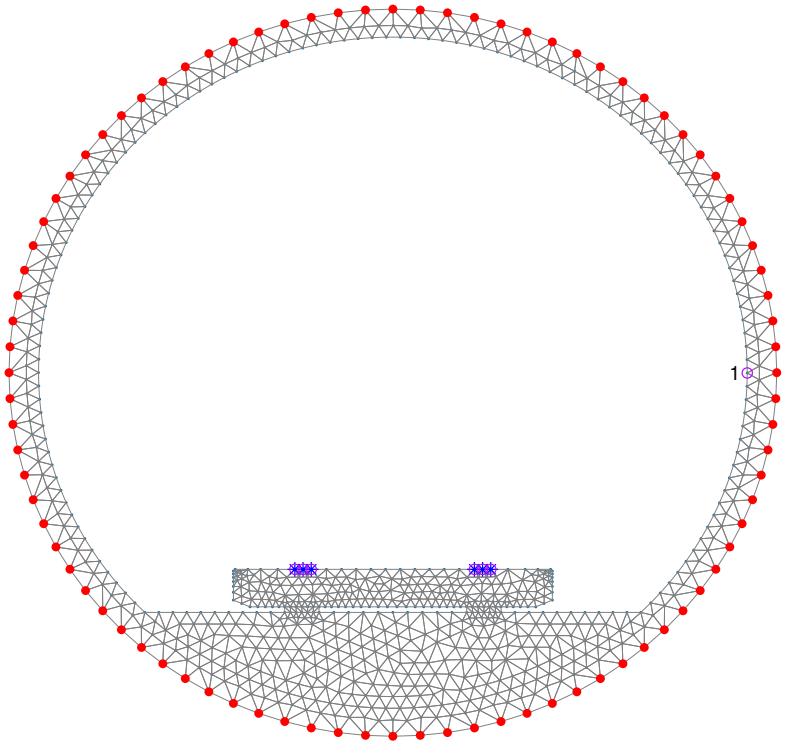

Fig. 5: Schematic of the FST system modelled by 2.5D FE (floating slab track and tunnel) and BE (soil). Red solid markers represent the BE nodes, blue star markers are the points where forces are applied and pink circular markers denote the evaluators, where the evaluator in the tunnel wall is denoted by 1.

semi-analytical solutions of a cylindrical cavity in a full-space are used to relate the displacement Green's functions in the tunnel/soil interface with the displacement and traction Green's functions in a set of evaluators in the soil used later for the energy flow computations. The properties of the soil are summarised in the Table 5. The evaluators in the soil are located at radial distances of 5 m from the outer wall of the tunnels (which represents a radial distance of 8.25 m from the centre of the tunnels) and placed at angular locations linearly distributed from $\theta = \pi/2$ rad to $\theta = \pi$ rad, and with 19 discrete points. Since the systems studied in this application study

Subsystem	Parameters	Units	Value
Tunnel	Young's modulus	[GPa]	3.5
	Poisson ratio	[−]	0.15
	Density	[kg/m^3]	2500
	Damping	[−]	0.01
Floating slab	Young's modulus	[GPa]	3.5
	Poisson ratio	[−]	0.15
	Density	[kg/m^3]	2500
	Damping	[−]	0.01
Elastomeric mat	Young's modulus	[MPa]	2.73
	Poisson ratio	[−]	0.35
	Density	[kg/m^3]	1328
	Damping	[−]	0.05

Table 3: Properties of FST.

Subsystem	Parameters	Units	Value
Rails	Density	[kg/m^3]	7850
	Young's modulus	[GPa]	207
	Cross-sectional area	[m^2]	$23.5 \cdot 10^{-6}$
	Second moment of inertia	[kg/m^2]	$6930 \cdot 10^{-6}$
Fasteners	Stiffness	[MN/m]	35
	Damping	[−]	$35{\cdot}10^3$

Table 4: Properties of the rails and fasteners used in DFF and FST.

are symmetric, the vibration energy radiated upwards can be computed multiplying by 2 the energy flow in the cylindrical strip defined by $\theta_1 = \pi/2$ rad and $\theta_2 = \pi$ rad.

Parameters	Units	Value
Density	[kg/m^3]	2191
Young's modulus	[MPa]	180
Poisson ratio	[−]	0.3
Damping	[−]	0.025

Table 5: Properties of soil.

The sampling strategy mentioned in section 2.3 is followed to obtain the response of the system modelled with the numerical methodology. A total of 2^9 samples of $\tilde{\omega}$ and 2^{11} samples of k_x are considered for both models. Once the required Green's functions of the system are obtained, the train/track interaction and the train pass-by models are applied to obtain the response in the evaluator 1 at the tunnel wall and at the evaluators of the soil. The train is composed by 5 cars, while the properties of each car are summarised in Table B.7. The linearised Hertz contact stiffness is computed for the present case, obtaining a value of $1.23 \cdot 10^9$ N/m. It is assumed that both rails have the same unevenness profile. The train speed in these simulations is assumed to be 25 m/s, which is a common speed of operation of metro trains.

4.1. Vibration analysis

In this section, the analysis of the vibration response of both tunnel systems due to train passage is performed. The response of the rail and the tunnel is obtained at the railhead (vertical response) and at evaluator 1 in the tunnel wall, respectively. Figure 6 shows the vibration acceleration response of the rails and evaluator 1 in the time domain for DFF and FST systems. Figure 7 shows the frequency content for the vertical component of the vibration acceleration of the rail and the evaluator on the tunnel wall in one-third octave bands for DFF and FST cases. The octave bands are normalised with respect to train pass time, which is computed as $(\tilde{x}_{N_a} - \tilde{x}_1)/v_t$.

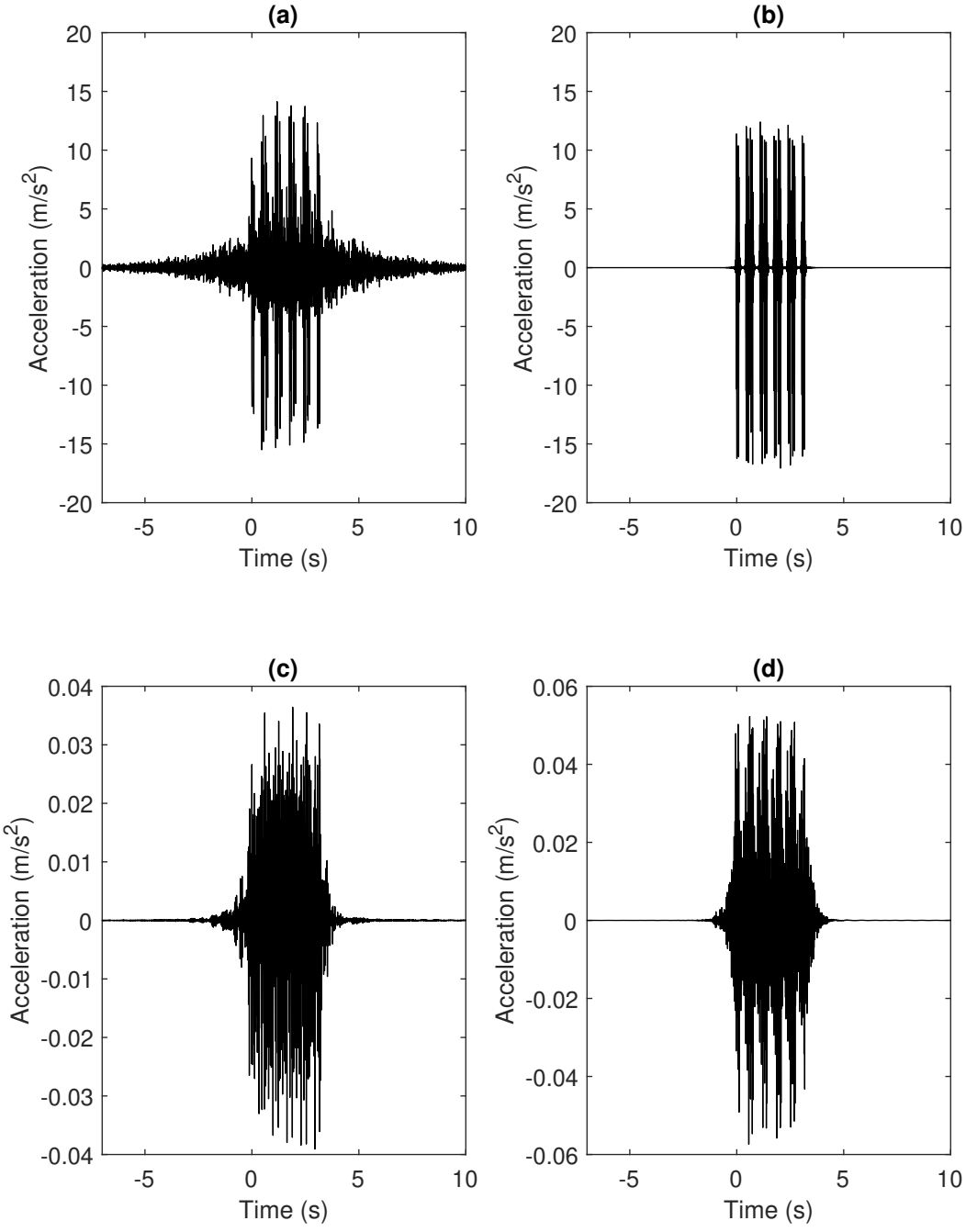

Fig. 6: Acceleration response in the time domain of the rail for the FST (a) and DFF (b) systems and on the evaluator 1 for the FST (c) and DFF (d) systems.

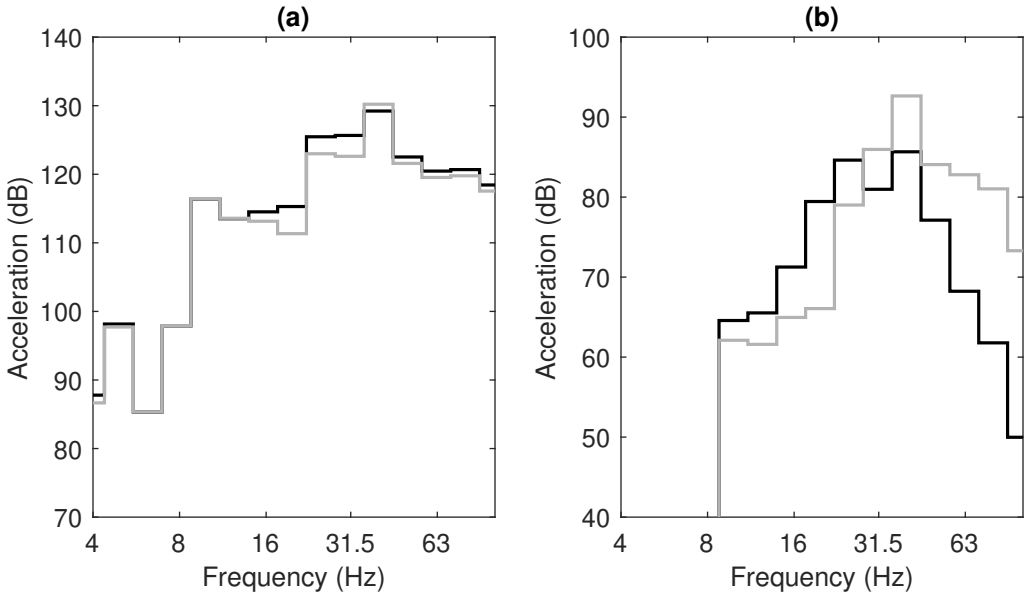

Fig. 7: One-third octave bands of the vertical acceleration spectrum of the rail (a) and the horizontal acceleration spectrum of the evaluator 1 (b). Solid black line represents the response of the FST system and solid grey line represents the DFF system response. The dB are computed with a reference of 10^{-6} m/s^2.

In Fig. 7, it can be seen that, in general, the level of vibration of the rail for the the FST system is larger that the one for the DFF system, mostly for the bands of 20 Hz, 25 Hz and 31.5 Hz. In contrast, it is shown that the level of vibration on the evaluator at the tunnel wall for the FST system is smaller and the frequency content is shifted to lower frequencies, inducing to large differences between the frequency responses of the FST and DFF systems at high frequencies, where the FST is reducing drastically the levels of vibration as compared with the DFF system. The reduction of the vibration levels at the tunnel wall can be also evaluated using the maximum transient vibration value (MTVV) as an indicator. It is obtained that the MTVV for DFF system is 0.0583 m/s^2 and for the FST system is 0.0308 m/s^2, which implies

a reduction of 5.5 dB. These results are in accordance with previous studies that compared these two types of track solutions [9, 41].

4.2. Vibration energy flow analysis

In this section, a detailed analysis of the vibration energy flow radiated by both tunnel systems considered in this application study is performed. For the vibration energy flow analysis, the total vibration energy flow, the energy spectral density and the energy spectrum radiated by DFF and FST are obtained. It is important to note that, in this case, the term energy is referred to the physical vibration energy and it should not be confused with the energy associated to a signal typically used in signal processing. The vibration energy flow analysis is performed on the evaluators in the soil previously mentioned.

$$E = r_m \int_{\theta_1}^{\theta_2} \int_{-\infty}^{\infty} \boldsymbol{v}(0,\theta,t) \cdot \boldsymbol{\tau}(0,\theta,t) \mathrm{d}t \mathrm{d}\theta. \tag{21}$$

Using Eq. (21), the total energy flow per meter radiated by both DFF and FST tunnel systems at distances of 5 m away from the outer tunnel wall is obtained and presented along with MTVV in the Table 6.

Track type	MTVV	Total vibration energy flow
DFF	0.0583 m/s^2	0.2547 J/m
FST	0.0308 m/s^2	0.2227 J/m

Table 6: Comparison of total energy flow from DFF and FST with MTVV of the vibration at the tunnel wall.

As can be seen, the FST has lower total vibration energy flow radiated upwards than DFF, which is the same trend as the one obtained with MTVV.

However, a comparison of the values of MTVV with total vibration energy flow shows that the amount of reduction obtained with FST based on total vibration energy flow (0.6 dB) is significantly less than that obtained by MTVV criterion (5.5 dB).

In order to analyse the disparity between total vibration energy flow and MTVV indicators, the energy spectral density (ESD) is proposed. Taking into account that the power flow radiated through the previously defined cylindrical strip is given by

$$P(t) = r_m \int_{\theta_1}^{\theta_2} \boldsymbol{v}(0,\theta,t) \cdot \boldsymbol{\tau}(0,\theta,t) \mathrm{d}\theta, \tag{22}$$

and accounting for the Parseval's theorem, the energy spectral density can be computed by the expression

$$\mathrm{ESD} = r_m \int_{\theta_1}^{\theta_2} \boldsymbol{V}(0,\theta,\omega) \cdot \boldsymbol{T}^*(0,\theta,\omega) \mathrm{d}\theta, \tag{23}$$

where $\boldsymbol{T}$ is the Fourier transform of $\boldsymbol{\tau}$ and $\boldsymbol{T}^*$ is complex conjugate of $\boldsymbol{T}$. Figure 8 shows the ESD and energy spectra (ES) in one third octave bands radiated by DFF and FST systems. In a similar way as the vibration analysis of the previous section pointed out, Fig. 8 shows that the FST system is shifting the frequency content to lower frequencies. However, in light of the total energy flow results previously obtained, one can see from Fig. 8 that the difference in ES values at higher frequencies of FST and DFF is not as much as compared with acceleration values in Fig. 7 (b). This is the reason for the observed disparity between the reduction obtained by MTVV and

vibration energy flow values. It should be noted that vibration energy flow takes into account the effect of stress (in the soil) which is not accounted in MTVV values.

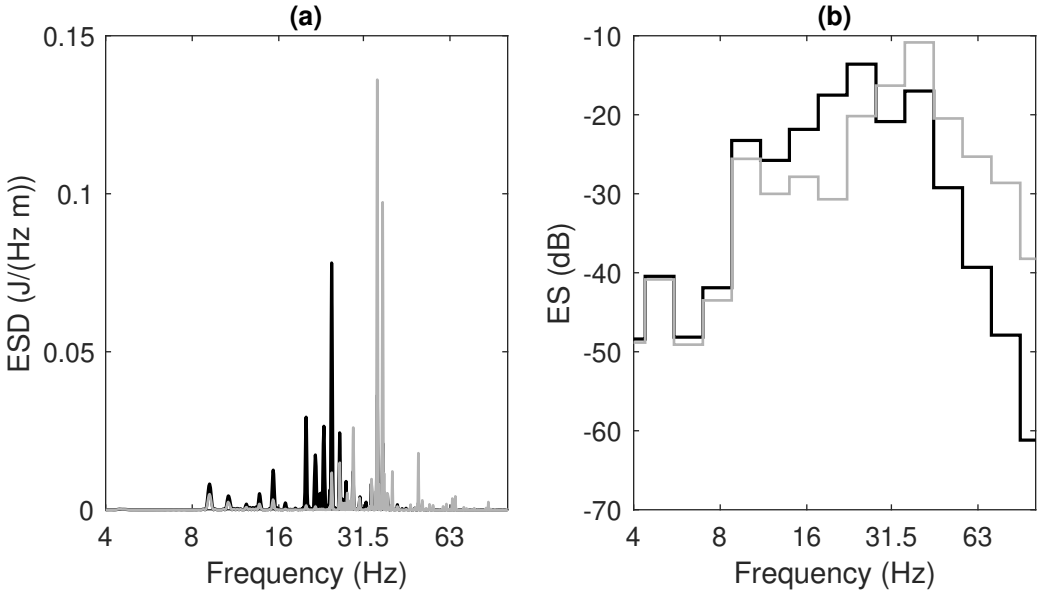

Fig. 8: ESD of the vibration energy flow radiated upwards (a) for the evaluators in soil located at a distance of 5 m the outer tunnel wall for the cases of the DFF system (solid grey line) and FST system (solid black line). ES in one-third octave bands bands of the vibration energy flow radiated upwards (b) for the evaluators in soil located at a distance of of 5 m the outer tunnel wall for the cases of the DFF system (solid grey line) and FST system (solid black line). The dB are computed with a reference of 1 J/m.

5. Conclusions

In this article, a methodology to compute the vibration energy flow in the soil from underground railway infrastructures due to railway traffic is presented. The methodology uses a 2.5D FEM-BEM approach to compute the response at the tunnel/soil interface and at other evaluators placed in the tunnel

structure. The track is modelled with a semi-analytical model consisting of two continuously supported Euler-Bernoulli beams as a model of the two rails and their fastening systems. Traction and displacement Green's functions inside the soil domain are obtained from the displacement Green's functions obtained on the track/soil interface using the semi-analytical solution of a cylindrical cavity in a full-space. 2D rigid multibody model of the train cars is used to obtain the train pass-by response of the track/tunnel/soil system. A new non-uniform sampling strategy for the wavenumber is proposed in this paper. This strategy aims to capture accurately the response of the system in the wavenumber-frequency domain. Strategies for fast computation of the BEM matrices are described. A methodology for fast computation of the Green's functions is also described and expressions of asymptotic solutions for 2.5D Green's functions of a full-space are presented in Appendix A.

A new perspective for the comparison of mitigation measures is given in the present paper based on vibration energy flow radiated upwards as an indicator. A comparison of two different underground railway infrastructures, one based on a floating-slab track (FST) and another one based on a direct fastening system track (DFF), is presented as an example of this new perspective. From the analysis of the induced vibration using MTVV criterion and using the vibration energy radiated for both case studies presented in the paper, it can be concluded that the FST system is a better vibration mitigation solution than DFF system. However, these two indicators are providing significantly different estimations of the insertion loss of the FST system as compared with the DFF one. This high discrepancy casts significant doubts on the methodology for assessing the vibration induced by underground rail-

way infrastructures based on only one accelerometer placed at the tunnel wall, which is the typical practice nowadays. Further work on this regard is required in order to get the complete picture of the comparison between these two indicators and also to provide a new methodology, probably based on a setup of various accelerometers located at the tunnel wall, that really represents the vibration energy that the tunnel system is emitting to the surroundings.

Acknowledgements

The present work is supported by the Ministerio de Economía y Competitividad under the research grant BES-2015-071453, individual research grant related to the project ISIBUR: Innovative Solutions for the Isolation of Buildings from Underground Railway-induced Vibrations supported by the Ministerio de Ciencia e Innovación, Retos de Investigación 2014, with reference TRA2014-52718-R. The authors want to also acknowledge the financial support provided by the project VIBWAY: Fast computational tool for railway-induced vibrations and re-radiated noise assessment, supported by the Ministerio de Ciencia e Innovación, Retos de Investigación 2018, with reference RTI2018-096819-B-I00. The second author also wants to acknowledge the funds provided by the NVTRail project, Noise and Vibrations induced by railway traffic in tunnels: an integrated approach, with grant reference POCI-01-0145-FEDER-029577, funded by FEDER funds through COMPETE2020 (Programa Operacional Competitividade e Internacionalização (POCI)) and by national funds (PIDDAC) through FCT/MCTES.

Appendix A. 2.5D static Green's functions for displacements and tractions for a homogeneous full-space

The full-space elastodynamic Green's functions for tractions and displacements for nonzero frequency can be found in [40]. In this section, analytical solutions of Green's displacements and stress are given for two cases: ($\omega = 0,\ k_x \neq 0$) and ($\omega = 0,\ k_x = 0$). The tractions Green's functions can be found from the stress Green's functions σ, which can be obtained from strains Green's functions using the relation $\sigma^k_{i,j} = \lambda\varepsilon^k_{vol}\delta_{i,j} + 2\mu\varepsilon^k_{i,j}$, where $i, j, k = \{x, y, z\}$. In this section, $H^{(2)}_n$ are n-th order Hankel's functions of the second kind, λ is the first Lamé constant, μ is the second Lamé constant, β is the S-wave speed, α is the P-wave speed, ρ is the density of the medium, $r = \sqrt{y^2 + z^2}$ and ν is the Poisson ratio of the medium.

Appendix A.1. Expressions of the displacements Green's functions for $k_x \neq 0$ and $\omega = 0$

$$
\begin{aligned}
G_{xx} &= \frac{H_0^{(2)}(\mathrm{i}k_x r)}{4\mathrm{i}\rho\beta^2} - \frac{k_x r H_1^{(2)}(\mathrm{i}k_x r)}{8\rho}\left(\frac{1}{\beta^2} - \frac{1}{\alpha^2}\right), \\
G_{yy} &= \frac{H_0^{(2)}(\mathrm{i}k_x r)}{4\mathrm{i}\rho\beta^2} - \frac{1}{4\mathrm{i}\rho}\left(\frac{1}{\beta^2} - \frac{1}{\alpha^2}\right)\left[\frac{H_0^{(2)}(\mathrm{i}k_x r)}{2}\right. \\
&\quad \left. - \frac{\mathrm{i}k_x r\gamma_y^2}{4}\left(H_1^{(2)}(\mathrm{i}k_x r) - H_3^{(2)}(\mathrm{i}k_x r)\right) - \gamma_y^2 H_2^{(2)}(\mathrm{i}k_x r)\right], \\
G_{zz} &= \frac{H_0^{(2)}(\mathrm{i}k_x r)}{4\mathrm{i}\rho\beta^2} - \frac{1}{4\mathrm{i}\rho}\left(\frac{1}{\beta^2} - \frac{1}{\alpha^2}\right)\left[\frac{H_0^{(2)}(\mathrm{i}k_x r)}{2}\right. \\
&\quad \left. - \frac{\mathrm{i}k_x r\gamma_z^2}{4}\left(H_1^{(2)}(\mathrm{i}k_x r) - H_3^{(2)}(\mathrm{i}k_x r)\right) - \gamma_z^2 H_2^{(2)}(\mathrm{i}k_x r)\right], \\
G_{xy} &= \frac{\gamma_y k_x r}{8\rho}\left(\frac{1}{\beta^2} - \frac{1}{\alpha^2}\right) H_0^{(2)}(\mathrm{i}k_x r), \\
G_{xz} &= \frac{\gamma_z k_x r}{8\rho}\left(\frac{1}{\beta^2} - \frac{1}{\alpha^2}\right) H_0^{(2)}(\mathrm{i}k_x r), \\
G_{yz} &= \frac{\gamma_z \gamma_y k_x r}{8\rho}\left(\frac{1}{\beta^2} - \frac{1}{\alpha^2}\right) H_1^{(2)}(\mathrm{i}k_x r).
\end{aligned} \tag{A.1}
$$

Appendix A.2. Expressions of the displacements Green's functions for $k_x = 0$ and $\omega = 0$

$$
\begin{aligned}
G_{xx} &= \frac{1}{8\pi(1-\nu)\mu}(3-4\nu)\ln\frac{1}{r}, \\
G_{yy} &= \frac{1}{8\pi(1-\nu)\mu}\left[(3-4\nu)\ln\frac{1}{r} - \gamma_y^2\right], \\
G_{zz} &= \frac{1}{8\pi(1-\nu)\mu}\left[(3-4\nu)\ln\frac{1}{r} - \gamma_z^2\right], \\
G_{xy} &= 0, \\
G_{yz} &= \frac{\gamma_y\gamma_z}{8\pi(1-\nu)\mu}, \\
G_{xz} &= 0.
\end{aligned} \tag{A.2}
$$

Appendix A.3. Expressions of the strains Green's functions for $k_x \neq 0$ and $\omega = 0$

In order to get obtain the strains for the case of $k_x \neq 0$ and $\omega = 0$, the terms presented in Eq. A.3 are derived for that case. Substituting this terms in the original equations presented by Tadeu and Kausel [40], it is possible to find

the strains for the case of $k_x \neq 0$ and $\omega = 0$.

$$
\begin{aligned}
A \cdot B_0 &= \frac{r}{16\mu(1-\nu)} \frac{H_1^{(2)}(\mathrm{i}k_x r)}{k_x}, \\
A \cdot B_1 &= \frac{-\mathrm{i}r}{16\mu(1-\nu)} H_0^{(2)}(\mathrm{i}k_x r), \\
A \cdot B_2 &= \frac{k_x r}{16\mu(1-\nu)} H_1^{(2)}(\mathrm{i}k_x r), \\
A \cdot B_3 &= \frac{\mathrm{i}k_x^2 r}{16\mu(1-\nu)} H_2^{(2)}(\mathrm{i}k_x r),
\end{aligned}
\tag{A.3}
$$

Appendix A.4. Expressions of the strains Green's functions for $k_x = 0$ and $\omega = 0$

$$
\begin{aligned}
\varepsilon^x_{\text{vol}} &= \varepsilon^x_{yy} = \varepsilon^x_{zz} = 0,\\
\varepsilon^x_{xy} &= -\frac{\gamma_y}{4\pi\rho\beta^2 r},\\
\varepsilon^x_{xz} &= -\frac{\gamma_z}{4\pi\rho\beta^2 r},\\
\varepsilon^x_{yz} &= 0,\\
\varepsilon^y_{\text{vol}} &= -\frac{\gamma_y}{2\pi\rho\alpha^2 r},\\
\varepsilon^y_{yy} &= \frac{\gamma_y}{4\pi\rho r}\left(\frac{1-2\gamma_y^2}{\beta^2} - \frac{3-2\gamma_y^2}{\alpha^2}\right),\\
\varepsilon^y_{zz} &= \frac{\gamma_y}{4\pi\rho r}(1-2\gamma_z^2)\left(\frac{1}{\beta^2} - \frac{1}{\alpha^2}\right),\\
\varepsilon^y_{xy} &= \varepsilon^x_{yy} = 0,\\
\varepsilon^y_{yz} &= -\frac{\gamma_z}{4\pi\rho r}\left(\frac{2\gamma_y^2}{\beta^2} + \frac{1-2\gamma_y^2}{\alpha^2}\right),\\
\varepsilon^z_{\text{vol}} &= \varepsilon^y_{\text{vol}},\\
\varepsilon^z_{yy} &= \frac{\gamma_z}{4\pi\rho r}(1-2\gamma_y^2)\left(\frac{1}{\beta^2} - \frac{1}{\alpha^2}\right),\\
\varepsilon^z_{zz} &= \frac{\gamma_z}{4\pi\rho r}\left(\frac{1-2\gamma_z^2}{\beta^2} - \frac{3-2\gamma_z^2}{\alpha^2}\right),\\
\varepsilon^z_{xy} &= \varepsilon^z_{xz} = 0,\\
\varepsilon^z_{yz} &= -\frac{\gamma_y}{4\pi\rho r}\left(\frac{2\gamma_z^2}{\beta^2} + \frac{1-2\gamma_z^2}{\alpha^2}\right).
\end{aligned}
\tag{A.4}
$$

Appendix B. Vehicle model

The vehicle model used in the present work is an extension of the one presented by Lei and Noda [42] considering massive springs as a model of the primary suspension. A summary of the parameters for this vehicle model, the values taken in the present paper and the units of each parameter are shown in Table B.7. As shown, the massive parameters are divided by two since the values required of the half-vehicle. The stiffness of the secondary and primary suspension are already given for of vehicle system.

Vehicle parameters	Notation	Units	Value
Car body mass	m_c	[kg]	41923/2
Car body mass inertia	J_c	[kg m^{-2}]	(9.17/2)·10^5
Sprung mass of the ith bogie	$m_{\text{bog}}^{s(i)}$	[kg]	720/2
Stiffness of the ith bogie's secondary suspension	$k_{ss}^{(i)}$	[N m^{-1}]	8.14·10^5
Structural damping coefficient of the ith bogie's secondary suspension	$\eta_{ss}^{(i)}$	[−]	0
Viscous damping of the ith bogie's secondary suspension	$c_{ss}^{(i)}$	[N s m^{-1}]	15·10^3
Unsprung mass of the ith bogie	$m_{\text{bog}}^{(i)}$	[kg]	1730/2
Unsprung mass inertia of the ith bogie	$J_{\text{bog}}^{(i)}$	[kg m^{-2}]	824/2
Stiffness of the jth wheelset's primary suspension	$k_{ps}^{(j)}$	[N m^{-1}]	1.24·10^6
Structural damping coefficient of the jth wheelset's primary suspension	$\eta_{ps}^{(j)}$	[−]	0

Viscous damping of the jth wheelset's primary suspension	$c_{ps}^{(j)}$	[N s m^{-1}]	$\cdot 10^4$
Mass of the jth wheelset's primary suspension	$m_{ps}^{(j)}$	[kg]	0
Mass of the jth wheelset	$m_w^{(j)}$	[kg]	1410/2
Distance between bogies of the same car	d_{sc}	[m]	11.368
Distance between bogies of different cars	d_{dc}	[m]	4.97
Distance between wheelsets of the ith bogie	$d_w^{(i)}$	[m]	2

Table B.7: Vehicle model parameters and data.

References

[1] ISO 2631-1, Mechanical vibration and shock. Evaluation of human exposure to whole-body vibration. Part 1: General requirements, International Organization for Standardization, 1997.

[2] G. Lombaert, G. Degrande, S. François, D. J. Thompson, Ground-Borne Vibration due to Railway Traffic: A Review of Excitation Mechanisms, Prediction Methods and Mitigation Measures, in: Noise and Vibration Mitigation for Rail Transportation Systems, volume 126, 2015, pp. 253–287.

[3] ISO 14837-1, Mechanical vibration. Ground-borne noise and vibration arising from rail systems. Part 1: General guidance, International Organization for Standardization, 2005.

[4] A. Dijckmans, A. Ekblad, A. Smekal, G. Degrande, G. Lombaert, Efficacy of a sheet pile wall as a wave barrier for railway induced ground vibration, Soil Dynamics and Earthquake Engineering 84 (2016) 55–69.

[5] A. Dijckmans, P. Coulier, J. Jiang, M. G. Toward, D. J. Thompson, G. Degrande, G. Lombaert, Mitigation of railway induced ground vibration by heavy masses next to the track, Soil Dynamics and Earthquake Engineering 75 (2015) 158–170.

[6] A. Castanheira-Pinto, P. Alves Costa, L. Godinho, P. Amado-Mendes, On the application of continuous buried periodic inclusions on the filtering of traffic vibrations: A numerical study, Soil Dynamics and Earthquake Engineering 113 (2018) 391–405.

[7] D. J. Thompson, J. Jiang, M. G. Toward, M. F. Hussein, A. Dijckmans, P. Coulier, G. Degrande, G. Lombaert, Mitigation of railway-induced vibration by using subgrade stiffening, Soil Dynamics and Earthquake Engineering 79 (2015) 89–103.

[8] P. Alves Costa, R. Calçada, A. Silva Cardoso, Ballast mats for the reduction of railway traffic vibrations. Numerical study, Soil Dynamics and Earthquake Engineering 42 (2012) 137–150.

[9] T. Balendra, K. H. Chua, K. W. Lo, S. L. Lee, Steady-state vibration

of subway-soil-building system, Journal of Engineering Mechanics 115 (1989) 145–162.

[10] T. Balendra, C. G. Koh, Y. C. Ho, Dynamic response of buildings due to trains in underground tunnels, Earthquake Engineering & Structural Dynamics 20 (1991) 275–291.

[11] K. H. Chua, T. Balendra, K. W. Lo, Groundborne vibrations due to trains in tunnels, Earthquake Engineering & Structural Dynamics 21 (1992) 445–460.

[12] X. Sheng, C. J. C. Jones, D. J. Thompson, Prediction of ground vibration from trains using the wavenumber finite and boundary element methods, Journal of Sound and Vibration 293 (2006) 575–586.

[13] H. E. M. Hunt, Prediction of vibration transmission from railways into buildings using models of infinite length, Vehicle System Dynamics 24 (1995) 234–247.

[14] H. E. M. Hunt, Modelling of rail vehicles and track for calculation of ground-vibration transmission into buildings, Journal of Sound and Vibration 193 (1996) 185–194.

[15] H. E. M. Hunt, Stochastic modelling of traffic-induced ground vibration, Journal of Sound and Vibration 144 (1991) 53–70.

[16] P. Fiala, G. Degrande, F. Augusztinovicz, Numerical modelling of ground-borne noise and vibration in buildings due to surface rail traffic, Journal of Sound and Vibration 301 (2007) 718–738.

[17] D. Clouteau, M. Arnst, T. M. Al-Hussaini, G. Degrande, Freefield vibrations due to dynamic loading on a tunnel embedded in a stratified medium, Journal of Sound and Vibration 283 (2005) 173–199.

[18] P. Fiala, S. Gupta, G. Degrande, F. Augusztinovicz, A numerical model for re-radiated noise in buildings, in: Noise and Vibration Mitigation for Rail Transportation Systems. In: Proceedings of 9th International Workshop on Railway Noise, Munich, Germany, 2007, volume 99, pp. 115–121.

[19] D. Clouteau, M. L. Elhabre, D. Aubry, Periodic BEM and FEM-BEM coupling - Application to seismic behaviour of very long structures, Computational Mechanics 25 (2000) 567–577.

[20] X. Sheng, C. J. C. Jones, D. J. Thompson, Modelling ground vibration from railways using wavenumber finite- and boundary-element methods, Proceedings of the Royal Society A: Mathematical, Physical and Engineering Sciences 461 (2005) 2043–2070.

[21] G. Lombaert, G. Degrande, Ground-borne vibration due to static and dynamic axle loads of InterCity and high-speed trains, Journal of Sound and Vibration 319 (2009) 1036–1066.

[22] P. Alves Costa, R. Calçada, A. Silva Cardoso, Track-ground vibrations induced by railway traffic: In-situ measurements and validation of a 2.5D FEM-BEM model, Soil Dynamics and Earthquake Engineering 32 (2012) 111–128.

[23] S. François, M. Schevenels, P. Galvín, G. Lombaert, G. Degrande, A 2.5D coupled FE-BE methodology for the dynamic interaction between longitudinally invariant structures and a layered halfspace, Computer Methods in Applied Mechanics and Engineering 199 (2010) 1536–1548.

[24] P. Galvín, S. François, M. Schevenels, E. Bongini, G. Degrande, G. Lombaert, A 2.5D coupled FE-BE model for the prediction of railway induced vibrations, Soil Dynamics and Earthquake Engineering 30 (2010) 1500–1512.

[25] Kausel, J. M. Roësset, Stiffness matrices for layered soils, Bulletin of the Seismological Society of America 71 (1981) 1743–1761.

[26] Q. Jin, D. J. Thompson, D. E. J. Lurcock, M. G. R. Toward, E. Ntotsios, A 2.5D finite element and boundary element model for the ground vibration from trains in tunnels and validation using measurement data, Journal of Sound and Vibration 422 (2018) 373–389.

[27] P. Lopes, P. Alves Costa, M. Ferraz, R. Calçada, A. S. Cardoso, Numerical modeling of vibrations induced by railway traffic in tunnels: From the source to the nearby buildings, Soil Dynamics and Earthquake Engineering 61-62 (2014) 269–285.

[28] P. Amado-Mendes, P. Alves Costa, L. M. Godinho, P. Lopes, 2.5D MFS-FEM model for the prediction of vibrations due to underground railway traffic, Engineering Structures 104 (2015) 141–154.

[29] A. Yaseri, M. H. Bazyar, S. Javady, 2.5D coupled FEM-SBFEM analysis

of ground vibrations induced by train movement, Soil Dynamics and Earthquake Engineering 104 (2018) 307–318.

[30] M. Hussein, H. Hunt, A power flow method for evaluating vibration from underground railways, Journal of Sound and Vibration 293 (2006) 667 – 679. Proceedings of the Eigth International Workshop on Railway Noise.

[31] J. Forrest, H. Hunt, A three-dimensional tunnel model for calculation of train-induced ground vibration, Journal of Sound and Vibration 294 (2006) 678 – 705.

[32] M. F. M. Hussein, H. E. M. Hunt, A numerical model for calculating vibration from a railway tunnel embedded in a full-space, Journal of Sound and Vibration 305 (2007) 401–431.

[33] M. Hussein, S. François, M. Schevenels, H. Hunt, J. Talbot, G. Degrande, The fictitious force method for efficient calculation of vibration from a tunnel embedded in a multi-layered half-space, Journal of Sound and Vibration 333 (2014) 6996–7018.

[34] A. Clot, J. Romeu, R. Arcos, S. R. Martín, A power flow analysis of a double-deck circular tunnel embedded in a full-space, Soil Dynamics and Earthquake Engineering 57 (2014) 1–9.

[35] A. Clot, J. Romeu, R. Arcos, An energy flow study of a double-deck tunnel under quasi-static and harmonic excitations, Soil Dynamics and Earthquake Engineering 89 (2016) 1–4.

[36] Y. B. Yang, H. H. Hung, A 2.5D finite/infinite element approach for modelling visco-elastic bodies subjected to moving loads, International Journal for Numerical Methods in Engineering 51 (2001) 1317–1336.

[37] D. Ghangale, A. Colaço, P. Alves Costa, R. Arcos, A methodology based on structural finite element method-boundary element method and acoustic boundary element method models in 2.5D for the prediction of reradiated noise in railway-induced ground-borne vibration problems, Journal of Vibration and Acoustics 141 (2019) 031011.

[38] D. C. Gazis, Three-dimensional investigation of the propagation of waves in hollow circular cylinders. I. Analytical foundation, The Journal of the Acoustical Society of America 31 (1959) 568–573.

[39] B. Noori, R. Arcos, A. Clot, J. Romeu, Control of ground-borne underground railway-induced vibration from double-deck tunnel infrastructures by means of dynamic vibration absorbers, Journal of Sound and Vibration 461 (2019) 114914.

[40] A. Tadeu, E. Kausel, Green's functions for two-and-a-half-dimensional elastodynamic problems, Journal of Engineering Mechanics (2000) 1093–1097.

[41] F. Cui, C. H. Chew, The effectiveness of floating slab track system - Part I. Receptance methods, Applied Acoustics 61 (2000) 441–453.

[42] X. Lei, N. A. Noda, Analyses of dynamic response of vehicle and track coupling system with random irregularity of track vertical profile, Journal of Sound and Vibration 258 (2002) 147–165.